WCCM V
Fifth World Congress on
Computational Mechanics
July 7–12, 2002, Vienna, Austria
Eds.: H.A. Mang, F.G. Rammerstorfer,
J. Eberhardsteiner

Finite Element Calculation of Wave Propagation and Excitation in Periodic Piezoelectric Systems

Manfred Hofer*, **Reinhard Lerch**

Department of Sensor Technology
University of Erlangen-Nuremberg, Paul-Gordan-Str. 5, D-91052 Erlangen, Germany
e-mail: manfred.hofer@lse.e-technik.uni-erlangen.de

Norman Finger, Günter Kovacs

EPCOS AG
Postfach 801709, D-81617 Munich, Germany

Joachim Schöberl, Ulrich Langer

Institute of Computational Mathematics
Johannes Kepler University Linz, Altenberger Str. 69, A-4040 Linz, Austria

Key words: Finite Element Calculation, Wave Propagation, Piezoelectricity, Periodicity

Abstract

Many sensors and actuators in technical systems consist of quasiperiodic structures which are constructed by successive repetition of a base cell. Typical examples are piezoelectric composites used as ultrasonic transducers or surface acoustic wave (SAW) devices utilized in telecommunication systems. The precise numerical simulation of such devices including all physical effects is currently beyond the capacity of high end computation. Therewith, we have to restrict the numerical analysis to the periodic substructure and have to introduce special boundaries to account for the periodicity.

Due to the fact, that wave propagation phenomena have to be considered for SAW applications the periodic boundary condition (PBC) has to be able to model each possible mode within the periodic structure. That means this condition must hold for each phase difference existing at the periodic boundaries. To fulfill this complex criteria we have introduced the Floquet theorem to the PBCs offering two different solution strategies: the first method leads to a quadratic eigenvalue problem. Therein, a huge matrix including all nodes not belonging to the periodic boundaries has to be inverted due to a Schur-Complement formulation. In the other method a general non symmetric eigenvalue problem including the inner and

the nodes at one periodic boundary has to be solved. These techniques consider every kind of propagating mode automatically. The advantage of the latter scheme is that the matrices keep sparse. With the use of an efficient eigensolver utilizing the Arnoldi method, which calculates only the needed eigenvalues and takes advantage of the sparsity of the matrices, the second approach is much faster as the scheme with the Schur-Complement which has to deal with dense matrices .
In the first part of this paper we describe the basic theory of our new PBC methods. In the second part we show simulation results for the eigensolution of a periodic SAW structure which can be expressed efficiently in a dispersion diagram. Such diagrams give valuable information to SAW designers such as wave velocity and reflectivity of electrodes and help them to better understand the interaction of surface acoustic waves (SAW) or leaky surface acoustic waves (LSAW) with radiating bulk waves. Finally, we calculate the charge distribution of SAW structures by solving the inhomogeneous piezoelectric partial differential equations with incorporated PBCs. Therewith, we determine the electrical admittance which characterizes the electrical behavior of a SAW device. Further on, the computation of a voltage excitation on arbitrary electrodes will be demonstrated using our newly developed PBCs.

1 Introduction

The aid of modern sensors and actuators made our life more comfortable in various ways: The heating controls the temperature itself with the aid of internal and external temperature sensors, irrigation is done automatically when the humidity sensor tells the control equipment that the soil is dry, movement sensors are used to switch on the front door light if somebody is appearing. There is a huge list of sensors and actuators which are used in modern “smart” homes [1]. On the other hand, modern sensors and actuators are used to increase our security. One of the most important example is the application of sensors in modern automobiles, e.g. slipping sensors used in tires which deliver the electronic stability program with input data or acceleration sensors which detect a collision with another car or another subject and enforces the control circuit to inflate the airbags.

The development of modern sensors is mostly done with simulation tools, because this way is much faster and cheaper compared with experimental measurements on prototypes. A very accurate method for this purpose is the finite element method (FEM) [2, 3, 4]. Therein, the real behavior of the transducers is approximated by partial differential equations (PDEs) which have to be discretized in space and time or frequency.
In many cases, a finite element simulation of a complete sensor is not possible, because the simulation time would be too large or the necessary computer resources would exceed the available amount. Therefore, the models have to be reduced in complexity or size by incorporating special properties or by neglecting features which contribute only in a diminutive way to the final output of the simulated device. Such complexity reduction can be done e.g. by regarding symmetry planes or by neglecting hysteresis effects or nonlinearities.

Many sensors, e.g. composite transducers [5] or SAW devices [6, 7] consist of periodic structures. This periodicity can be used to reduce the size of the FE model tremendously. In this paper, two different methods regarding the wave propagation in periodic structures are described in detail. A special focus will be given on periodic SAW structures.

2 Surface Acoustic Wave (SAW) Devices

A surface acoustic wave device consists of a piezoelectric substrate carrying metallic structures such as interdigital transducers (IDTs) and reflecting gratings or electrodes (see Fig. 1) [7]. Such SAW devices

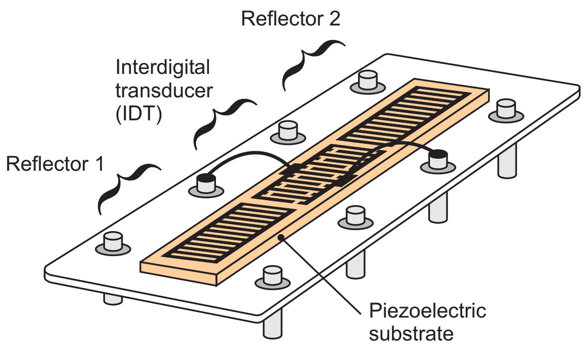

Figure 1: Sketch of a SAW resonator filter with an interdigital transducer (IDT) and two reflectors

are mainly used in telecommunications, e.g. as delay lines in television sets, intermediate frequency filters for mobile phones or convolvers for spread-spectrum communications [8]. They are also used in different sensor applications, e.g. for measuring temperature and pressure [9], flow [10] or humidity [11].

The working principle of a SAW device is illustrated in Fig. 2. A time harmonic voltage excitation of

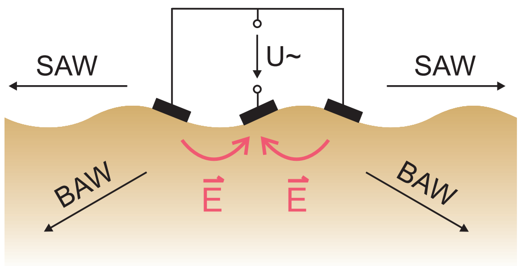

Figure 2: Working principle of a SAW device, generation of surface- and bulk acoustic waves (BAW)

the electrodes of an IDT leads to a deformation of the surface due to the inverse piezoelectric effect [12]. Depending on the excitation frequency, various wave modes are excited, e.g. surface acoustic waves or bulk acoustic waves (BAWs). On the other hand, due to the direct piezoelectric effect, surface displacements lead to a voltage in the electrodes and therewith, the surface strain can be transformed back into an electrical signal.

Typical SAW devices like SAW reflector filters may consist of up to thousands of electrodes, especially if they are built on piezoelectric substrates with low electromechanical coupling coefficient K^2 like quartz [7]. Therefore, a FEM simulation of a complete device is not possible due to the size of the evolving finite element grid. By regarding the periodic structure, the FEM model can be reduced to a manageable size.

3 Wave Propagation in Periodic Structures

A general periodic structure can be imagined as successive repetition of a base cell Ω_p (see Fig. 3). In the

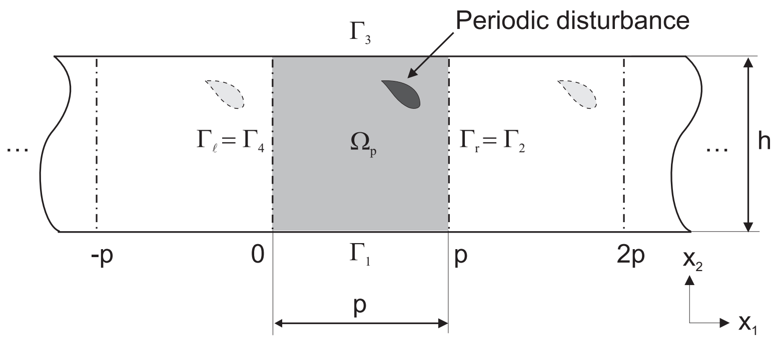

Figure 3: Base cell Ω_p with periodicity p

following, the boundary Γ_4 of Fig. 3 will be referred to as "left periodic boundary (Γ_l)" and boundary two (Γ_2) will be termed as "right periodic boundary (Γ_r)".

The main goal of our examination is to simulate arbitrary waves propagating in periodic structures. Therefore, it is not sufficient to restrict the results to waves with wavelengths λ of a fraction of twice the width p of the base cell ($\lambda = 2\,\mathrm{p}/i$ with $i \in \mathbb{N}^+$). These modes could be easily achieved by setting the degrees of freedom of the right periodic boundary Γ_r equal to those on Γ_l ($i = 2n$ with $n \in \mathbb{N}^+$), or to the negative of those from Γ_l ($i = 2n+1$ with $n \in \mathbb{N}_0$) [13, 14]. This kind of periodicity cannot be used if arbitrary waves have to be considered. Therefore, a more fundamental approach has to be pursued.

Due to the periodicity of the geometry, the resulting field distribution must be also quasi-periodic, leading to

$$u(x+p)e^{j\omega t} = u(x)e^{-\gamma p}e^{j\omega t} \;, \tag{1}$$

with u denoting the field distribution and $\gamma = \alpha + j\beta$ the complex propagation constant. The variable α describes the decay behavior and β stands for the phase propagation constant of the wave. In general, a time harmonic excitation is assumed. Therefore, the term $e^{j\omega t}$ will be omitted further on.
With a periodic function $u_p(x+p) = u_p(x)$, eq. (1) can be written as

$$u(x) = u_p(x)e^{-\gamma p} \;. \tag{2}$$

Expanding this periodic function in a Fourier series

$$u_p(x) = \sum_{m=-\infty}^{\infty} a_m e^{-j\frac{2\pi m}{p}x} \tag{3}$$

with a_m as Fourier coefficient, the complete field distribution can be written as superposition of damped, plane waves

$$u(x) = \sum_{m=-\infty}^{\infty} a_m e^{-\left(\gamma + j\frac{2\pi m}{p}\right)x} \;. \tag{4}$$

3.1 Dispersion diagram

It is important to know the relation between the complex propagation constant γ and the frequency ω to be able to describe wave propagation in periodic structures. This dependency can be illustrated in a so called dispersion diagram (Fig. 4).

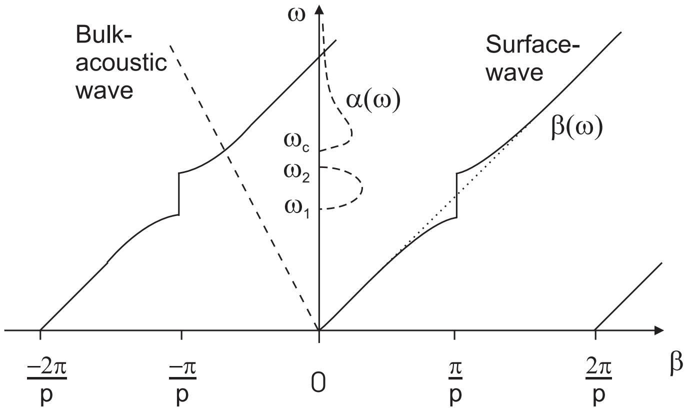

Figure 4: Dispersion diagram of a periodic structure

In general, two different regions can be distinguished:

- **Wave propagation:** At frequencies below the lower stopband edge ω_1 and above the upper stopband edge ω_2 the considered modes are propagating ones. At the onset-frequency ω_c a conversion to backscattered bulk waves occurs. This results in loss of energy of the propagating wave manifesting in a nonzero, positive damping coefficient α.

- **Wave reflection:** At frequencies in the stopband ($\omega_1 < \omega < \omega_2$) the waves are reflected at periodic disturbances (like electrodes) existing in the simulation area. These reflections add coherently, therefore, no propagating modes exist and the waves are damped exponentially ($\alpha > 0$ at $\beta = (2n+1)\pi/p$ with $n \in \mathbb{Z}$). The width of the stopband is proportional to the reflection per disturbance [15]. If no disturbance is present, the stopband vanishes (dotted line in Fig. 4).

4 FE Formulation of the Periodic Boundary Conditions (PBCs)

The fundamental equations for the FE simulation of piezoelectric media has been published many times. Therefore, our derivation directly starts at the FE matrix form of a harmonic piezoelectric problem [16]

$$\underbrace{\begin{pmatrix} \mathbf{K}^{uu} + j\omega\mathbf{C}^{uu} - \omega^2\mathbf{M}^{uu} & \mathbf{K}^{u\phi} \\ \mathbf{K}^{\phi u} & -\mathbf{K}^{\phi\phi} \end{pmatrix}}_{\mathbf{K}^\star} \begin{pmatrix} \mathbf{d} \\ \phi \end{pmatrix} = \begin{pmatrix} \mathbf{F} \\ \mathbf{Q} \end{pmatrix}, \tag{5}$$

where the notation has been chosen to

$\mathbf{M}^{uu}$	mechanical mass matrix
$\mathbf{C}^{uu}$	mechanical damping matrix
$\mathbf{K}^{uu}$	mechanical stiffness matrix
$\mathbf{K}^{\phi\phi}$	dielectric stiffness matrix
$\mathbf{K}^{u\phi}$	piezoelectric coupling matrix
$\mathbf{F}$	nodal vector of external mechanical forces
$\mathbf{Q}$	nodal vector of electric charges
$\mathbf{d}$	vector of mechanical displacements
ϕ	vector of electric potentials

For convenience, the matrix $K^\star$ has been introduced as combination of all FE matrices. In further deductions, the vector of unknowns will be denoted as $\mathbf{u}$ ($\mathbf{u} = [\mathbf{d}, \phi]^T$) and the source term on the right-hand-side as $\mathbf{R}$ ($\mathbf{R} = [\mathbf{F}, \mathbf{Q}]^T$). These definitions allow us to write (5) as

$$\mathbf{K}^\star \mathbf{u} = \mathbf{R} \; . \tag{6}$$

4.1 Schur-Complement Method

To be able to incorporate the periodicity condition (1) we split the unknowns $\mathbf{u}$ into inner nodes $\mathbf{u}_i$ and boundary nodes $\mathbf{u}_b$ ($\mathbf{u}_b = [\mathbf{u}_l, \mathbf{u}_r]$). The same has to be done with the matrix $\mathbf{K}^\star$ and the right-hand-side vector $\mathbf{R}$

$$\begin{pmatrix} \mathbf{K}^\star_{ii} & \mathbf{K}^\star_{ib} \\ \mathbf{K}^\star_{bi} & \mathbf{K}^\star_{bb} \end{pmatrix} \begin{pmatrix} \mathbf{u}_i \\ \mathbf{u}_b \end{pmatrix} = \begin{pmatrix} 0 \\ \mathbf{R}_b \end{pmatrix} . \tag{7}$$

The forces in the interior of the simulation area stay in equilibrium. Therefore, the right hand vector contributing to the inner nodes is a zero vector. This fact can be used to take the Schur-Complement of (7) resulting in

$$\underbrace{(-\mathbf{K}^\star_{bi}\mathbf{K}^{\star-1}_{ii}\mathbf{K}^\star_{ib} + \mathbf{K}^\star_{bb})}_{\mathbf{S}}\, \mathbf{u}_b = \mathbf{R}_b \; , \tag{8}$$

which can also be written as

$$\begin{pmatrix} \mathbf{S}_{ll} & \mathbf{S}_{lr} \\ \mathbf{S}_{rl} & \mathbf{S}_{rr} \end{pmatrix} \begin{pmatrix} \mathbf{u}_l \\ \mathbf{u}_r \end{pmatrix} = \begin{pmatrix} \mathbf{R}_l \\ \mathbf{R}_r \end{pmatrix} . \tag{9}$$

Incorporation of the periodicity condition (1) by replacing $\mathbf{u}_r$ with $\gamma \mathbf{u}_l$ and $\mathbf{R}_r$ with $-\gamma \mathbf{R}_l$ (the minus sign is required for the equilibrium of the appearing forces on the periodic boundaries) results in a quadratic eigenvalue problem in $\eta = e^{-\gamma p}$

$$\eta^2 \mathbf{S}_{lr}\mathbf{u}_l + \eta(\mathbf{S}_{ll} + \mathbf{S}_{rr})\mathbf{u}_l + \mathbf{S}_{rl}\mathbf{u}_l = 0 \; . \tag{10}$$

This equation can be solved for example by inverse iteration [17], with a two-sided Lanczos method [18], or by linearizing the system [19] which doubles the matrix size. The latter solution method is straight forward to implement and therein the standard non-symmetric eigenvalue solver from LAPACK [20] can be used.

The matrices in (10) are dense but very small: the size is proportional to the number of unknowns of one periodic boundary. Due to the Schur-Complement, an inversion of the matrix $\mathbf{K}^\star_{ii}$, which contains the unknowns of all inner nodes and is therefore of notable size, has to be performed. $\mathbf{K}^\star_{ii}$ includes the frequency weighted mass and damping matrices and thus, the inversion has to be performed for every frequency step separately.

4.2 Transformation to General Linear Eigenvalue Problem

A different scheme can be developed by starting at an equivalent formula to (7)

$$\underbrace{\begin{pmatrix} \mathbf{K}^\star_{ii} & \mathbf{K}^\star_{il} & \mathbf{K}^\star_{ir} \\ \mathbf{K}^\star_{li} & \mathbf{K}^\star_{ll} & \mathbf{K}^\star_{lr} \\ \mathbf{K}^\star_{ri} & \mathbf{K}^\star_{rl} & \mathbf{K}^\star_{rr} \end{pmatrix}}_{\mathbf{K}^\star} \begin{pmatrix} \mathbf{u}_i \\ \mathbf{u}_l \\ \mathbf{u}_r \end{pmatrix} = \begin{pmatrix} 0 \\ \mathbf{R}_l \\ \mathbf{R}_r \end{pmatrix}, \tag{11}$$

and incorporating the periodicity condition (1) in a similar way as before yields

$$\begin{pmatrix} \mathbf{K}^\star_{ii} & \mathbf{K}^\star_{il} & \mathbf{K}^\star_{ir} \\ \mathbf{K}^\star_{li} & \mathbf{K}^\star_{ll} & \mathbf{K}^\star_{lr} \\ \mathbf{K}^\star_{ri} & \mathbf{K}^\star_{rl} & \mathbf{K}^\star_{rr} \end{pmatrix} \underbrace{\begin{pmatrix} \mathbf{I}_i & 0 \\ 0 & \mathbf{I}_l \\ 0 & \gamma \mathbf{I}_l \end{pmatrix}}_{\mathbf{T}_1} \begin{pmatrix} \mathbf{u}_i \\ \mathbf{u}_l \end{pmatrix} = \begin{pmatrix} 0 \\ 1 \\ -\gamma \end{pmatrix} \mathbf{R}_l \tag{12}$$

with $\mathbf{I}$ denoting the identity matrix. Multiplication with an appropriate matrix from the left side eliminates the right hand side. The term with the squared propagation constant γ^2 cancels out because the according matrix $\mathbf{K}^\star_{rl}$ is per definition a zero matrix. Finally, the problem can be written as a general eigenvalue problem

$$\mathbf{A} \begin{pmatrix} \mathbf{u}_i \\ \mathbf{u}_l \end{pmatrix} = \gamma \mathbf{B} \begin{pmatrix} \mathbf{u}_i \\ \mathbf{u}_l \end{pmatrix} \tag{13}$$

with matrices

$$\mathbf{A} = \begin{pmatrix} \mathbf{K}^\star_{ii} & \mathbf{K}^\star_{il} \\ \mathbf{K}^\star_{ri} & 0 \end{pmatrix} \tag{14}$$

$$\mathbf{B} = \begin{pmatrix} 0 & -\mathbf{K}^\star_{ir} \\ -\mathbf{K}^\star_{li} & -(\mathbf{K}^\star_{ll} + \mathbf{K}^\star_{rr}) \end{pmatrix}. \tag{15}$$

These matrices are sparse but much larger compared with those from the Schur-Complement method. Here, all nodes of the interior of the simulation area and additionally those on one periodic boundary contribute to the matrices $\mathbf{A}$ and $\mathbf{B}$. At present, the sparsity of the matrices cannot be used due the lack of an eigenvalue solver for sparse, non-symmetric, complex matrices. In the future, Arnoldi methods will be used to solve our problems.
With our LAPACK solver the Schur-Complement method is much faster as the other method. Beside the calculation velocity both methods are equal and deliver same results.

4.3 Solution with Defined Excitation

With the above methods, all possible freely propagating modes can be calculated as eigenvalues of the described eigensystems. These give the SAW device designer valuable insight in general propagation properties of the special chosen configuration and materials.
In addition to freely propagating modes (= homogeneous solutions of the system of PDEs) one is also interested in particular solutions describing the excitation properties of the system: Here, the magnitude potential on the electrodes is fixed to a predefined value. Assuming a phase difference of θ from unit cell to unit cell, the propagation constant takes the form $\gamma = j\beta = j\theta/p$. Since, in this case, both ω and β are given, only a quite simple system of linear equations has to be solved. In principle, the matrices of both

methods (the Schur-Complement method and the transformation to general linear eigenvalue problem) can be applied, but the Schur-Complement needs an additional matrix inversion and therefore the faster transformation method will be utilized.
For the SAW designer it's important to know the charge distribution at an electrode. With the aid of the SAW part of the Green's function, one is able to calculate the excited waves of a SAW structure [6].

5 Results

A typical example for wave propagation in SAW structures has been chosen to show the functionality of our methods (see. Fig. 5). The simulations and measurements have been performed on a substrate

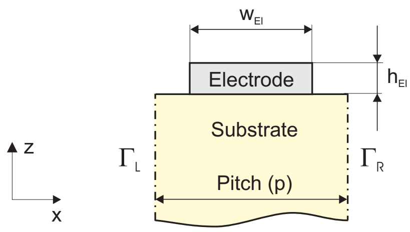

Figure 5: Model for the simulation of wave propagation in periodic SAW structures

of 37.5° rotated quartz with aluminum electrodes. The material constants have been taken from [21]. The height of the electrode w_{El} was fixed at 250 nm, the pitch p at $4\,\mu m$ and the metalization ration η ($\eta = w_{El}/p$ with w_{El} the electrode width) has been varied to show the influence of the electrode width on the propagation properties, like stopband edge and stopband width. The substrate hight was chosen to be eight pitches.
As an example, the propagation diagram of a SAW structure with a metalization ration of $\eta = 0.5$ can be seen in Fig. 6(a). The measured data are slightly beneath the simulated ones. This can be explained

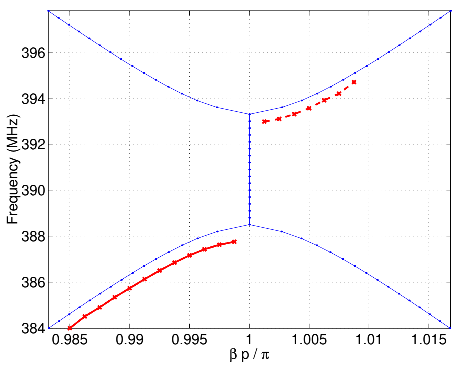

(a) Exemplary dispersion diagram at $\eta = 0.5$

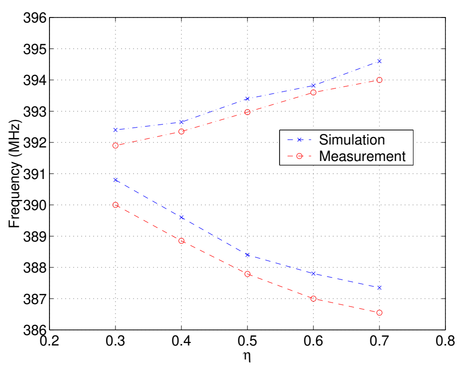

(b) Stopband edges as a function of metalization ratio η

Figure 6: Comparison of simulation and measurement of SAW structures on 37.5° rotated quartz

with the finite simulation area. With increasing depth of the simulated substrate, the solution converges

against the measured results, because the i-th approximated eigenvalue is bounded from below by the i-th exact eigenvalue while Galerkin rules are not violated (e.g. when reduced integration is employed) [3]. This fact has experimentally proofed by simulations with a substrate height of only four pitches. In this case, the stopband edges raise approximately 2 MHz at a total stopband width of about 5 Mhz.
Various metalization ratios have been examined with our method (Fig. 6(b)). Measurements are possible only outside the stopband, therefore, the measured data have been extrapolated to the value $\beta p/\pi = 1$ to obtain the measured stopband width for this comparison. The influence of the electrode width on the stopband size mainly due to the additional mass loading [22] can be recognized clearly.
The model in Fig. 5 has also been used to calculate the charge distribution on the electrode (see Fig. 7).

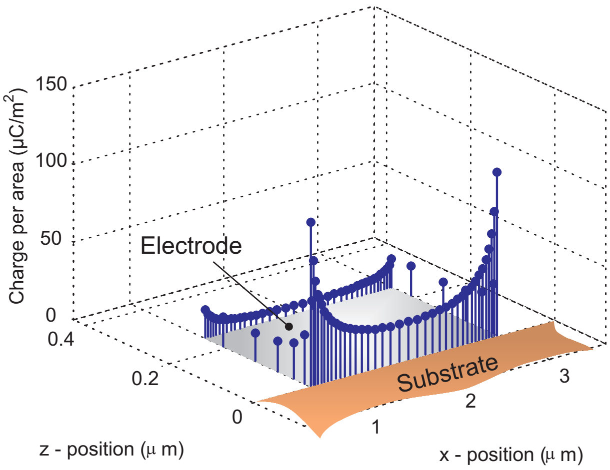

Figure 7: Charge distribution at an aluminum electrode

For the calculation of the charge distribution at all electrode edges, the air around the electrode has to be taken into account. In air, the electric potential has to be calculated but the mechanical field may be neglected due to the extremely low mechanical stiffness of the surrounding air. The only thing to be regarded is the vanishing stress contribution on the free substrate surface. Especially for materials with low dielectric constants (relative dielectric constants of quartz: $\varepsilon_{r_{xx}} = 4.5$ and $\varepsilon_{r_{zz}} = 4.6$) the surface charge of the electrode-air interfaces has to be taken into account. The charge on these interfaces can be estimated by $1/\varepsilon_r$ times the charge of the electrode-substrate interface. Calculating the total charge at electrodes on a quartz substrate one would make an error of at least 16% by neglecting the charge on the electrode-air interfaces.
The calculated total charge at the electrode with varying phase difference can be regarded as a kind of frequency spectrum. From this dependency, the so called “harmonic admittance” Y ($Y = j\omega Q/U$ with Q the total charge and U the electrical excitation potential) can be calculated (Fig. 8(a)) [23]. The little “disturbances” in the harmonic admittance coincide exactly with propagating modes calculated as eigenvalues of the system. In addition to the modes occurring in real SAW devices, spurious plate modes can be seen due to the Dirichlet boundary condition on the bottom of the FE model. With the aid of absorbing boundary conditions for piezoelectric materials, these spurious modes can be eliminated.
At angles a few degrees beside 180° bulk acoustic waves are excited. They can be recognized as a nonzero real part of the harmonic admittance. To be able to see this effect in the harmonic admittance, absorbing boundary conditions are needed again. Another possibility to simulate bulk acoustic waves correctly is the use of analytical solutions at the bottom boundary instead of Dirichlet conditions [24].

With the inverse discrete Fourier transformation it is possible to calculate the field distribution for an excitation at arbitrary electrodes, e.g. at only one "hot" electrode finger of a SAW one port resonator from the harmonic admittance.
The charge distribution on the electrode-substrate interface as a function of the phase angle θ can be seen in Fig. 8(b). For angles near to $180°$ the electrode potential of neighboring electrodes have a different sign. Therefore, the charges on different electrodes attract each other. They concentrate mainly at the electrode edges. On the other hand, at angles near $0°$ or $360°$ neighbored electrodes have nearly the same potential. Thus, the attraction is not as strong and the charge is distributed more uniformly over the electrode width.

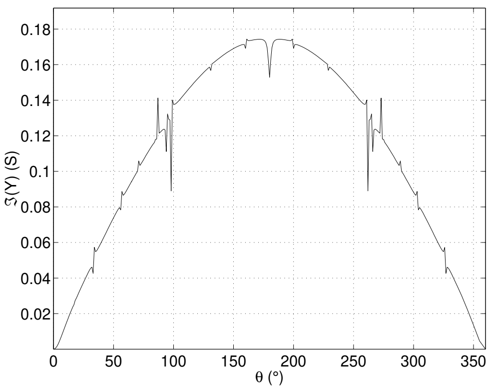

(a) Imaginary part of the harmonic admittance $\Im(Y)$

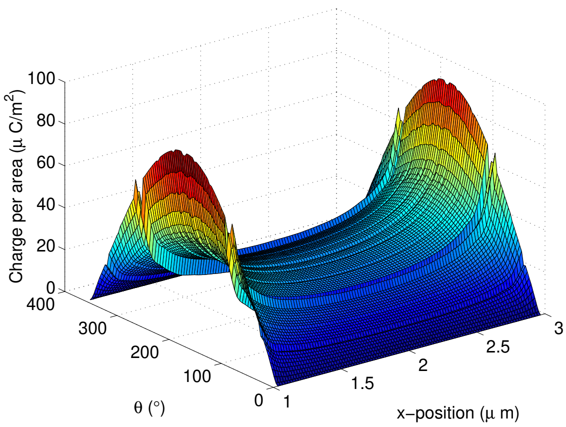

(b) Charge distribution on the interface of electrode and substrate

Figure 8: Imaginary part of the harmonic admittance Y respectively the charge distribution in an electrode as a function of the phase θ between left and right boundary ($\eta = 0.5$, $f = 390\,\text{MHz}$)

6 Conclusion

Two different finite element methods for the calculation of wave modes in periodic piezoelectric configurations like surface acoustic wave (SAW) structures have been introduced. The first method results in a quadratic eigenvalue problem with small, dense matrices. The second approach leads to a general linear eigenvalue problem with large, sparse matrices. The resulting complex eigenvalues can be interpreted as propagation and damping constants of the according mode.
With given phase angle between left and right boundary of a base cell of the periodic structure and the electrical potential on the SAW electrodes, the complete charge distribution at the electrode can be calculated. With the aid of the SAW part of the Green's function, this charge distribution can be used to calculate the complete propagation modes. Due to the finite simulation area and the Dirichlet boundary condition at the bottom of the simulation area, spurious plate modes appear in the charge distribution. They can be eliminated either with the introduction of absorbing boundary conditions or the use of analytical solutions at the bottom boundary. These methods will be examined in the next future.

References

[1] O. Gaussmann, H. Meixner, eds., *Sensors in Intelligent Buildings*, vol. 2 of *Sensors Application*, Wiley-VCH, Weinheim (2001).

[2] K. Bathe, *Finite Element Procedures*, Prentice-Hall, New Jersey (1996).

[3] T. Hughes, *The Finite Element Method*, Prentice-Hall, New Jersey, 1 edn. (1987).

[4] O. Zienkiewicz, *The Finite Element Method*, McGraw-Hill, New York, 4 edn. (1994).

[5] A. Safari, G. Sa-gong, J. Giniewicz, R. Newnham, *Composite Piezoelectric Sensors*, in *Proceedings of the 21st University Conference on Ceramic Science* (1986), pp. 445–454.

[6] D. P. Morgan, *Surface-Wave Devices for Signal Processing*, vol. 19 of *Studies in Electrical and Electronic Engineering*, Elsevier (1991).

[7] C. K. Campbell, *Surface Acoustic Wave Devices*, Applications of Modern Acoustics, Acacdemic Press, San Diego (1998).

[8] K. Hashimoto, *Surface Acoustic Wave Devices in Modern Communication Systems and their Simulation Technologies*, Springer, Berlin (2000).

[9] G. Schimetta, F. Dollinger, G. Scholl, R. Weigel, *Wireless Pressure and Temperature Measurement Using a SAW Hybrid Sensor*, in *IEEE Ultrasonic Symposium Proceedings* (2000), pp. 445–448.

[10] S. G. Joshi, *Flow Sensor Using Surface Acoustic Waves*, in *IEEE Ultrasonic Symposium Proceedings* (1988), pp. 555–558.

[11] J. D. N. Cheeke, N. Tashtoush, N. Eddy, *Suface Acoustic Wave Humidity Sensor Based on the Changes in the Viscoelastic Properties of a Polymer film*, in *IEEE Ultrasonic Symposium Proceedings* (1996), pp. 449–452.

[12] W. G. Cady, *Piezoelectricity*, Dover Publications, New York (1964).

[13] M. Buchner, W. Ruile, A. Dietz, R. Dill, *FEM Analysis of the Reflection Coefficient of SAWs in an Infinite Periodic Array*, in *IEEE Ultrasonics Symposium Proceedings* (1991), pp. 371–375.

[14] Y.-K. Yong, *Analysis of Periodic Structures for BAW and SAW Resonators*, in *IEEE Ultrasonics Symposium Proceedings* (2001), to be published.

[15] D.-P. Chen, H. A. Haus, *Analysis of Metal-Strip SAW Gratings and Transducers*, IEEE Transactions on Sonics and Ultrasonics, 32(3), (1985), 395–408.

[16] R. Lerch, *Simulation of Piezolectric Devices by Two- and Three-Dimensional Finite Elements*, IEEE Trans. Ultrasonics, Ferroelectrics and Frequency Control, 37(3), (1990), 233–247.

[17] A. Y. Leung, *Inverse Iteration for the Quadratic Eigenvalue Problem*, Journal of Sound and Vibration, 124(2), (1988), 247–267.

[18] C. Rajakumar, *Lanczos Algorithm for the Quadratic Eigenvalue Problem in Engineering Applications*, Computer Methods in Applied Mechanics and Engineering, 105, (1993), 1–22.

[19] D. Afolabi, *Linearization of the Quadratic Eigenvalue Problem*, Computers and Structures, 26(6), (1987), 1039–1040.

[20] E. Anderson, Z. Bai, C. Bischof, S. Blackford, J. Demmel, J. Dongarra, J. D. Croz, A. Greenbaum, S. Hammarling, A. McKenney, D. Sorensen, eds., *LAPACK Users' Guide*, SIAM, 3 edn. (1999).

[21] B. A. Auld, *Acoustic Fields and Waves in Solids*, vol. 1, Krieger Publishing Company, Inc., Florida, 2 edn. (1990).

[22] C. Dunnrowicz, F. Sandy, T. Parker, *Reflection of Surface Waves from Periodic Discontinuities*, in *IEEE Ultrasonic Symposium Proceedings* (1996), pp. 386–390.

[23] V. P. Plessky, S. V. Biryukov, J. Koskela, *Harmonic Admittance and Dispersion Equations - The Theorem*, IEEE Transactions on Ultrasonics, Ferroelectrics and Frequency Control, 49(4), (2002), 528–533.

[24] A. Isobe, M. Hikita, K. Asai, *Propagation Characteristics of Longitudinal Leaky SAW in Al-Grating Structure*, IEEE Transactions on Ultrasonics, Ferroelectrics and Frequency Control, 46(4), (1999), 849–855.